Raman scattering, defect luminescence, and phonon spectra of ^{7}LiH, ^{6}LiH, and ^{7}LiD crystals

Anthony Anderson* and Fritz Lüty
Department of Physics, University of Utah, Salt Lake City, Utah 84112
(Received 14 March 1983)

Two types of phonon spectra, obtained by Ar^+-ion-laser irradiation of lithium hydride crystals, have been observed and analyzed for the three isotopic components ^{6}LiH, ^{7}LiH, and ^{7}LiD. Two-phonon Raman spectra of pure crystals were measured at 300 and 10 K. One-phonon spectra were obtained from measurements of the resolved sideband structure of a strong zero-phonon emission line around 600 nm. This emission is produced by defects of very weak electron-phonon coupling, which are present in crystals either irradiated or containing a slight nonstoichiometric excess of Li. Both Raman and luminescence spectra show in their detailed resolved structure pronounced isotope shifts allowing a classification of the phonon modes involved. Comparison with data from neutron scattering and lattice-dynamics calculations gives very close agreement and identifies the modes as originating essentially from X and L points at the Brillouin-zone edges. Isotope effects on the zero-phonon lines of the defect luminescence are also observed and discussed.

I. INTRODUCTION

Lithium hydride provides, besides interesting material properties (such as the highest density form of hydrogen storage), several outstanding qualities for scientific studies:

(a) With only four electrons in the primitive cell it is the *simplest ionic solid* in terms of electronic structure. Both cations and anions have *closed-shell $1s^2$ configurations like He atoms.*

(b) *Isotope exchange* in both cation and anion sublattices allows by far *the largest relative mass variation* among all ionic solids.

Both these features make LiH crystals very attractive for studies of solid-state properties, such as lattice dynamics, intrinsic electron excitation, defect properties, etc. Well-established experimental results with sizable isotope effects in this simple electronic structure can provide prototypical model cases for the theory, e.g., for testing lattice-dynamics or defect computations. Ultimately, these simple ionic solids are prime candidates for first-principles calculations—for example, the theoretical derivation of lattice dynamics from electronic properties.[1]

In spite of these attractive features, work on LiH crystals has been somewhat limited, particularly when compared to the abundantly studied alkali halides. In a series of classical papers in the early 1960's, Pretzel and coworkers at Los Alamos described the preparation and main properties of LiH crystals and studied various irradiation induced defects.[2] In spite of an extended phenomenological collection of optical and EPR spectra, basically no well-secured microscopic defect models could be derived. (Even the assignment of the F center to an optical absorption is still controversial.) Systematic doping studies are essentially missing. Infrared absorption[3] and reflectivity[4] as well as elastic constant[5] measurements have been reported, and shell-model calculations[6] of the effective charge have been performed and compared to experiments. Results from neutron[7,8] and second-order Raman[9] measurements have been used, with good success, as a basis for lattice-dynamics calculations.[8,9] Only the H→D isotope variation, however, was exploited in these studies. A first parameter-free microscopic theory for the lattice dynamics of an ionic crystal was applied to the calculation of phonon dispersion curves of LiD as a test case, yielding good agreement at least in the acoustic branches.[10]

We have started a program toward a systematic defect study in these materials, in which highly pure, as well as systematically doped, materials, modern tools such as Raman spectroscopy, and the full possibilities of isotope exchange are being applied. In the first report we establish the light scattering and emission properties of the "pure" materials, extending the earlier second-order Raman work by including the ^{6}LiH case. We originally planned to proceed from there to doped or irradiated crystals, attempting to obtain for the first time defect-induced one-phonon Raman spectra and their isotope effects. It turned out, however, that even the pure compounds already contained defects with interesting optical behavior, which had to be studied first. These defects—too low in concentration for optical absorption or Raman detection—show up under visible laser light excitation by a strong optical emission at low temperature. The weak electron-phonon coupling of the defects results in a very strong zero-phonon emission line accompanied by essentially a one-phonon sideband spectrum. The resolved structure of the latter—very similar to a Raman spectrum—allows comparison with results from lattice-dynamics calculations and neutron scatterings. The pronounced isotope effects on the frequencies of both the intrinsic two-phonon and extrinsic one-phonon spectra, observed in ^{6}LiH, ^{7}LiH, and ^{7}LiD, turn out to be a very powerful tool in classifying the various modes and assigning their origin to particular points in the Brillouin zone.

II. EXPERIMENTAL TECHNIQUES AND MATERIALS

The raw material for the crystal growth was synthesized by gradual heating of Li metal under isobaric hydrogen in tungsten crucibles, *in situ* in the crystal-growth chamber. The purities and sources of the elemental materials are as follows: natural lithium ($\geq$99.99% chemically pure, 92.6% ^{7}Li), Electronic Space Products, Inc., Los Angeles; enriched lithium ($\geq$99.99% chemically pure, 95.58% ^{6}Li), Oak Ridge National Laboratories; hydrogen ($\geq$99.99% chemically pure), Whitmore Oxygen Co., Utah; and deuterium ($\geq$99.99% chemically pure, 99.5% ^{2}H), Matheson Company, Newark, California.

Single-crystal boules of ^{7}LiH, ^{6}LiH, and ^{7}LiD, typically 2 cm in diameter and 5 cm long, were grown by the Czochralski technique in the Utah Crystal Growth Laboratory. The crystals were readily cleavable along the [100] planes. Virgin crystals had a slightly blue-grey color, which can be attributed to nonstoichiometric excess of lithium present during the growth cycle. On annealing for several days at 500°C under $\sim$3 atm of hydrogen or deuterium, this color, which as will be discussed later, was directly related to the observed luminescence, could be almost completely eliminated. It was also found that exposing the annealing samples to moderate doses ($\sim$100 μC) of $\sim$1 MeV electrons from a Van der Graaf accelerator restored the color and luminescence.

Small freshly cleaved samples, about $5\times3\times1$ mm^3, were used for the optical measurements. They were mounted on the tail section of a variable flow cryostat and could be maintained at temperatures between 10 and 300 K by using liquid helium and nitrogen.

Spectra were excited by various lines of an argon-ion laser (Spectra Physics, Model 171), particularly those at 514.5 and 488.0 nm. Powers between 50 mW and 2 W were used, depending on the intensity of the emitted signals. Radiation from the crystals was dispersed in a double grating spectrometer (Spex, Model 1402), detected with a thermoelectrically cooled photomultipler (RCA C31034), and analyzed with photon counting electronics (Ortec, Model 9315), with output to an X-Y recorder.

III. EXPERIMENTAL RESULTS

Crystals with the rock-salt structure exhibit no first-order Raman phonon spectra because the crystal has inversion symmetry about every host-lattice ion. However, second-order spectra, involving combinations of phonons throughout the Brillouin zone, may be readily observed. In the case of lithium hydride, these spectra extend over a wide frequency range (up to 2500 cm^{-1}) and show considerable structure. In Figs. 1 and 2 typical spectra of ^{6}LiH, ^{7}LiH, and ^{7}LiD, at 300 and 10 K, respectively, are shown.

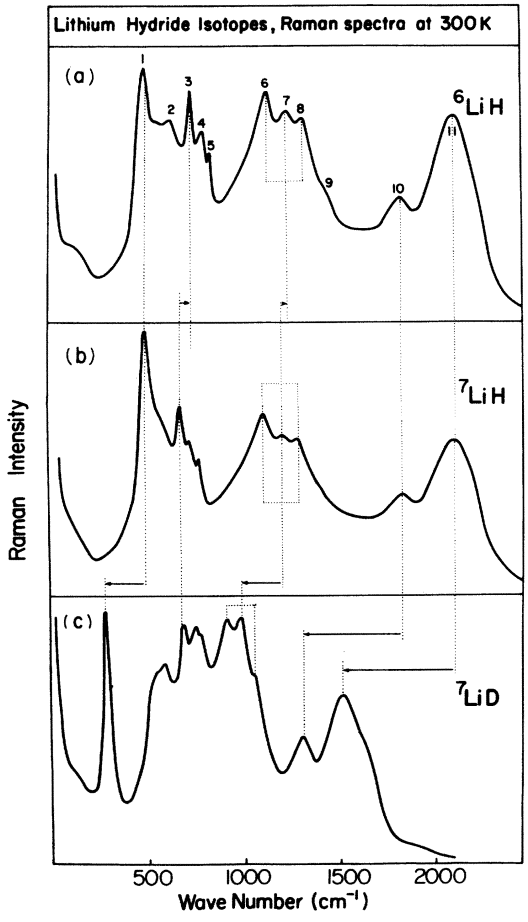

FIG. 1. Raman spectra of lithium hydride isotopes at 300 K.

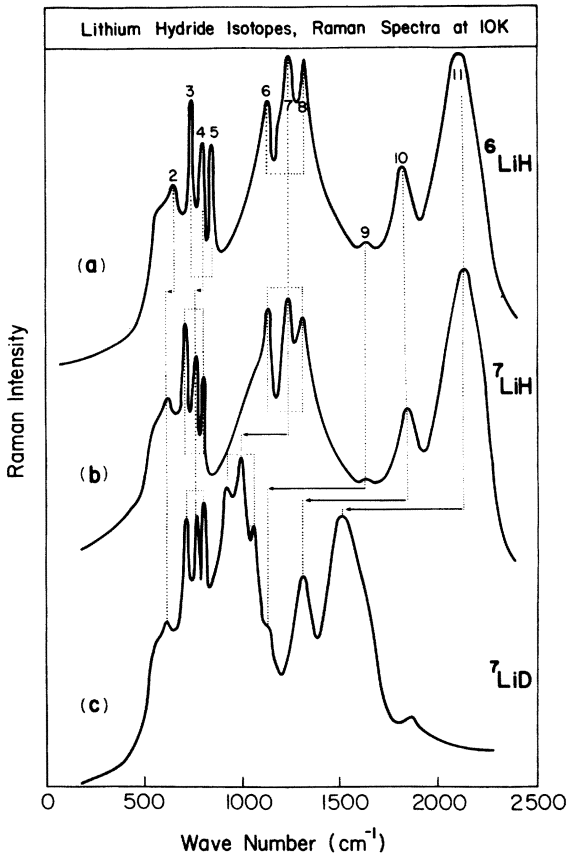

FIG. 2. Raman spectra of lithium hydride isotopes at 10 K.

The spectra have many obvious similarities, and corresponding peaks for the different isotopes have been indicated by dotted lines. It is seen that the spectra at 10 K are somewhat shifted ($\sim$20–40 cm^{-1}) to higher energies and show better resolution (reduced peak widths) compared to the room-temperature (RT) spectra. An additional feature observed at the higher temperature is the appearance of a strong peak (labeled no. 1 in Fig. 1) at lower frequencies. The loss of intensity of this peak as the temperature is lowered identifies it as a difference mode (hot band), and results from a depopulation of the lower-energy state involved in the combination.

The small peak observed at $\sim$1870 cm^{-1} in the LiD spectrum (Fig. 2) has no corresponding counterpart in the LiH spectra. It has been observed in earlier work[11] and interpreted to arise from a local mode of H^- defects in LiD, calculated to lie at $\nu_L = 917$ cm^{-1}, and expected to appear in Raman scattering at 2ν. We will not consider it further in this work.

In Table I frequencies of the 11 observed peaks in the two-phonon spectra of the three crystals are listed, together with their corresponding ratios. In the right-hand column, we have labeled corresponding frequencies according to one of five categories. These are based on isotopic mass dependencies and will be discussed in the next section.

During the Raman measurements under Ar^+ laser excitation, further sharp spectral features were observed at high-wave-number shifts. Variation of the exciting laser lines preserved the absolute spectral position of these emissions, identifying them as a luminescence effect. The strength of this emission was found to be correlated to the blue-grey color of the crystals caused by nonstoichiometric excess of Li. By long-time annealing of the crystal under H_2 or D_2 atmosphere, the luminescence signal essentially vanished together with the color of the crystal. After short exposure to electron irradiation at RT both the color and the luminescence spectra could be restored. Variation among the available Ar^+ laser lines (between 454 and 514 nm) revealed a steady increase of the luminescence intensity under excitation tuning to longer wavelengths.

At the lowest temperature reached (10 K), the emission shows greatest strength and the simplest spectral structure, consisting of a strong zero-phonon line accompanied by a phonon-sideband spectrum. Figure 3 displays for the three isotopic compounds the spectral position of the sharp emission line and the spectral shape of its sidebands. The frequency difference of the sideband peaks from the zero-phonon line and their ratios for the different isotopic components are summarized in Table II.

At 10 K the peak intensity of the sharp line emission is about 30 times stronger than the peak intensity of the sideband spectrum. [Count rates as high as 10^6 per second were recorded for the zero-phonon line with spectrometer slits at their narrowest setting (10 μm) and laser powers as low as 50 mW]. The width of the zero-phonon line is ap-

TABLE I. Two-phonon Raman peaks (numbers 1–11) of ^{6}LiH, ^{7}LiH, and ^{7}LiD crystals at 300 and 10 K.

Peak[a] number	Temperature (K)	Observed frequencies (cm^{-1}) (a) ^{6}LiH	(b) ^{7}LiH	(c) ^{7}LiD	Frequency ratios (a)/(b)	(b)/(c)	(a)/(c)	Type[b]
1	300	486	508	284	0.956	1.789	1.711	*D*
	10	np[c]	np[c]	np[c]				
2	300	631	589	591	1.071	0.997	1.068	*B*
	10	660	611	617	1.080	0.990	1.070	
3	300	731	685	695	1.067	0.986	1.052	*B*
	10	753	704	711	1.070	0.990	1.059	
4	300	786	739	753	1.064	0.981	1.044	*B*
	10	821	767	772	1.070	0.994	1.063	
5	300	825	776	795	1.063	0.976	1.038	*B*
	10	857	802	804	1.069	0.998	1.066	
6	300	1121	1108	907	1.012	1.222	1.236	*E* or *C*
	10	1153	1134	917	1.017	1.237	1.257	
7	300	1228	1206	968	1.018	1.246	1.269	*E* or *C*
	10	1257	1241	1000	1.013	1.241	1.257	
8	300	1309	1289	1049	1.016	1.229	1.248	*E* or *C*
	10	1346	1324	1059	1.017	1.250	1.271	
9	300	nr[d]	nr[d]	nr[d]				*A*
	10	1662	1671	1125	0.995	1.485	1.477	
10	300	1814	1832	1305	0.990	1.404	1.390	*A*
	10	1849	1876	1317	0.986	1.424	1.404	
11	300	2087	2109	1495	0.990	1.411	1.396	*A*
	10	2136	2151	1508	0.993	1.426	1.416	

[a]See Figs. 1 and 2 for labeling of peaks.
[b]See Sec. IV (discussion) and Table III for basis of classification.
[c]Not present.
[d]Not resolved.

proximately 5 cm^{-1}, which means that the integrated sharp line and the integrated total sideband emission are roughly of the same order of magnitude.

Under temperature increase to ~80 K, the zero-phonon line intensity decreases drastically (~a factor of 100), becoming comparable in strength to the sideband spectrum which decreases itself by approximately a factor of 5. Together with this decrease, several new sharp lines and new broad emission features appear which become more prominent than the original low-temperature emission. Apparently, a photochemical conversion or an energy transfer from the defect responsible for the 10 K emission occurs to other defects with slightly different spectral emission properties. As we were interested in this work essentially for the analysis of the phonon spectra, we did not follow up on these interesting transformations of defect emissions, leaving this to future work.

IV. DISCUSSION

A. Two-phonon Raman spectra

The spectra in this work are in good agreement with those from a previous polarized Raman study[9] on ^{7}LiH and ^{7}LiD, though of higher resolution and improved signal-to-noise ratio. In addition, the frequencies corresponding to maxima in the two-phonon spectrum of ^{6}LiH provide valuable information for identifying the form of the modes. No polarization properties were investigated in the present work.

In order to help categorize the observed peaks, we have calculated the expected frequency ratios for the three different lithium hydride isotopes, according to the basic types of modes at the Brillouin-zone center and edges. These are summarized in Table III. For type-*A* modes, the frequencies are inversely proportional to the square root of the proton or deuteron mass, and for type-*B* modes, to the square root of the lithium-ion mass. Type-*C* modes correspond to antiphase motion of the two ions at the zone center with frequencies varying inversely as the square root of the reduced mass, $\mu = M_H M_{Li}/(M_H + M_{Li})$. We have also calculated the ratios for difference and sum modes (types *D* and *E*, respectively), using the simplifying assumption that the force-constant dependence is identical for each of the combining modes (types *A* and *B*) and therefore cancels. This is strictly true only for a linear-chain nearest-neighbor model[12] but should approximate the behavior at the *L* point of the Brillouin zone for a crystal with the rock-salt structure.

As seen in Table I, the observed frequency ratios for the three isotopes fall into distinct groupings. Those at high frequencies correspond to hydrogen motions (*A* type), those at low frequencies to lithium motions (*B* type), and those at intermediate frequencies to either reduced-mass modes (*C* type) or a combination of *A* and *B* types. The latter is considered more likely, since the experimental ratios are slightly closer, and zone-edge modes appear to be more involved than zone-center ones in the two-phonon spectra. This is certainly true for the difference bands (no. 1 in Fig. 1) mentioned earlier and observed only at higher temperatures. Their frequency ratios at first sight seem to be anomalous, with $\nu(^6\text{LiH}):\nu(^7\text{LiH})$ *less* than unity and $\nu(^7\text{LiH}):\nu(^7\text{LiD})$ much greater than $\sqrt{2}$. The "inverse" effect for the lithium isotopes may be readily explained. The higher-frequency (*A*-type) mode is the same for both crystals, whereas the *B*-type mode is higher for ^{6}LiH. Hence the *difference (A-B)* is larger for ^{7}Li, as observed. Similar arguments may be used to explain the value for the LiH:LiD ratio.

The surprising simplicity of these categorizations implies that two-phonon transitions involving more complex modes (which would give frequency ratios other than those described in Table III) do not contribute appreciably to the Raman intensity—at least not to the resolved and detailed spectral structure. Secondly, it appears that zone-edge modes, where one or the other type of ion is stationary, are responsible for the major resolved features of the observed spectra.

These findings, based on straightforward mass-dependence arguments, can be confirmed and extended by a detailed comparison of the observed spectra with inelastic neutron scattering data[7] and with lattice-dynamic calculations.[8,9] We shall concentrate on a comprehensive theoretical treatment by Verble, Warren, and Yarnell[8] based on a seven-parameter shell model fitted to neutron data on ^{7}LiD. In Table IV calculated frequencies at the Γ,

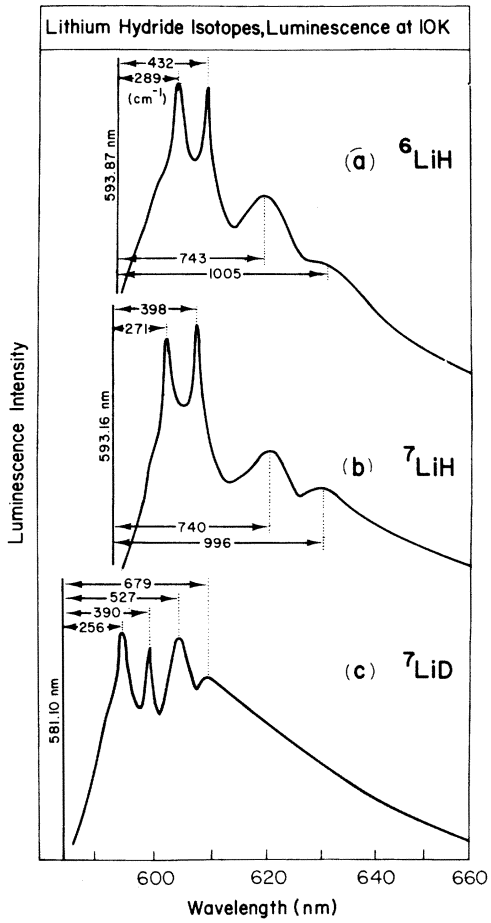

FIG. 3. Defect luminescence spectra of lithium hydride isotopes at 10 K.

TABLE II. Defect luminescence spectra of ^{6}LiH, ^{7}LiH, and ^{7}LiD crystals at 10 K.

Luminescence peak[a]	Observed frequencies[b] (cm^{-1}) (a) ^{6}LiH	(b) ^{7}LiH	(c) ^{7}LiD	Frequency ratios (a)/(b)	(b)/(c)	Mode type
Zero-phonon line	16839 (λ=593.87 nm)	16859 (λ=593.16 nm)	17209 (λ=581.10 nm)	0.999	0.980	
Phonon sideband 1	289	271	256	1.07	1.06	*B*
Phonon sideband 2	432	398	390	1.09	1.02	*B*
Phonon sideband 3	743	740	527	1.00	1.40	*A*
Phonon sideband 4	1005	996	679	1.01	1.47	*A*

[a]See Fig. 3 for labeling of peaks.

[b]Frequencies are absolute for zero-phonon lines; for the phonon sidebands, frequencies are expressed as displacements from the zero-phonon lines on the Stokes (low-frequency) side.

X, and *L* points of the Brillouin zone for ^{7}LiH and ^{7}LiD are listed. (These have been read from the graphs presented in Ref. 8.) We also show frequency ratios and note that differences between these and corresponding entries in Table III for mode types *A*, *B*, and *C* are minimal. This indicates that at both zone-edge points, *X* and *L*, the modes involve, predominantly, motion of one ion (hydrogen for the LO and TO modes, *A* type; and lithium for the LA and TA modes, *B* type). This is expected for the *L* point, since the (111) direction is perpendicular to alternate layers of anions and for this case the calculated frequency ratio (1.40) is indeed most close to $\sqrt{2}$. Even for the *X*-point modes, however, involving motions within ⟨100⟩ layers containing both cations and anions, the calculated frequency ratio (1.39) indicates very predominant contribution from the hydrogen motion.

In Table V we have used the values at the *X* and *L* points from Table IV to calculate the frequencies of various combinations of TO, TA, LO, and LA modes and compare them with the observed two-phonon Raman peaks for ^{7}LiH and ^{7}LiD. In general, the agreement is very satisfactory, especially for the lower-frequency peaks. The discrepancies at higher frequencies may result, at least partially, from limitations of the theory,[8] since no neutron data were available to fit the LO branches.

B. Defect luminescence

As our main interest in this work is directed at the detection and analysis of phonon-spectra and their isotope effects, we discuss this aspect of the observed defect luminescence at first, while treating other features only peripherally and later. The defect in question shows in emission a sharp zero-phonon line and a low-energy sideband spectrum—both having roughly equal integrated strength at low temperatures. This implies in linear electron-phonon coupling theory[13] a very weak coupling with a Huang-Rhys factor of $S \approx 1$. The emission transition at low temperatures occurs from the $n=0$ vibrational state of the electronic excited state with about equal strength into the $n=0$ and $n=1$ vibrational state of the electronic ground state. The sideband spectrum, measured in its displacement from the $0 \rightarrow 0$ purely electronic transition, reveals, very similarly to a Raman spectrum, the distribution and coupling strengths of phonon frequencies which couple to the electronic transition of the defect.

The observed sideband spectra (Fig. 3) reveal four distinct peaks which show pronounced isotope effects. From the frequency ratios of corresponding peaks for the three isotopes, listed in Table II, it is seen that the same classification of mode types is applicable as for the two-phonon Raman spectrum. The two higher-frequency bands correspond to hydrogen motion only (mode type *A*), and the two lower-frequency bands to lithium motion only (mode type *B*). In Fig. 4 the luminescence sideband spectra for ^{7}LiH and ^{7}LiD have been replotted on a wave-number scale and compared with the phonon density-of-states curves obtained from lattice-dynamic calculations.[8] Also indicated, by vertical lines, are the frequencies at the zone center (Γ point) and edges (*X* and *L* points), obtained from Table IV (which were read from the graphs in Ref. 4). As seen, there is very close agreement, indicating that the main features of the sideband spectra correspond to maxima in the phonon density-of-states curves, which in turn relate to the zone-edge frequencies. Apparently, the defect in question introduces only in a negligible way local force-constant changes, so that it acts as an ideal "local probe" for the detection of unperturbed lattice phonons.

The spectral contributions to the sideband spectra at energies beyond the one-phonon density (Fig. 4) are contributions from higher-order ($n=2$) phonon excitations.

TABLE III. Calculated frequency ratios of LiH isotope components for different types of modes.

Mode type	Description of mode	Calculated frequency ratios for (a) ^{6}LiH, (b) ^{7}LiH, (c) ^{7}LiD (a)/(b)	(b)/(c)	(a)/(c)
A	H motion only	1.00	1.41	1.41
B	Li motion only	1.08	1.00	1.08
C	Reduced-mass motion	1.01	1.33	1.35
D	Difference: $A-B$	0.95	1.89	1.80
E	Sum: $A+B$	1.01	1.28	1.30

TABLE IV. Calculated frequency values and ratios for Γ, X, and L point phonons of ^{7}LiH and ^{7}LiD (from Ref. 8).

Phonon branch	Calculated phonon frequencies (cm^{-1}) (b) ^{7}LiH Γ	X	L	(c) ^{7}LiD Γ	X	L	Calculated frequency ratios (b)/(c) Γ	X	L
LO	1080	937	968	812	672	689	1.33	1.39	1.40
TO	606	821	749	457	589	535	1.33	1.39	1.40
LA	0	392	569	0	396	586		0.99	0.97
TA	0	286	244	0	285	251		1.00	0.97

Qualitatively, it can be seen in Fig. 4 that these contributions, relative to the one-phonon spectrum, are stronger in LiD compared to LiH. This is an expected effect: The coupling parameter S, representing the order of the most probable phonon transition, depends on the mean value of the phonon frequencies, and therefore should depend on isotope variation. This predicted isotope effect,[13] which is normally extremely small, has never been observed. The large variation in the mean phonon frequencies of LiH and LiD make this effect easily observable, causing a higher ratio of the second- to first-order phonon spectrum for LiD compared to LiH.

Not only the phonon effects in the sidebands but also the purely electronic transitions, as seen in the sharp zero-phonon lines (ZPL), exhibit distinct and interesting isotope effects. The position ν of the ZPL is shifted, both by

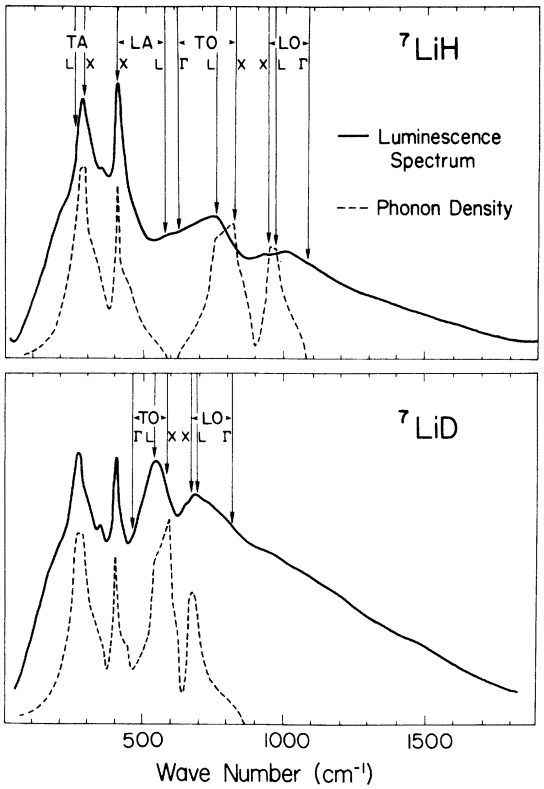

FIG. 4. Sideband luminescence spectra, phonon density-of-states curves, and frequency positions of Γ-, L-, and X-point phonons for ^{7}LiH and ^{7}LiD. The X- and L-point TA and LA frequencies, which remain unchanged under H→D isotope variation, are left out of the lower figure for clarity.

^{6}Li→^{7}Li substitution ($\Delta\nu/\nu = +1.2\times10^{-3}$), and by H→D substitution ($\Delta\nu/\nu = +2\times10^{-2}$). Isotope shifts of electronic transitions can, in principle, be caused either by a *static* effect (due to changes in lattice parameter) or by a *dynamic* effect (due to changes in the quadratic terms of the electron-phonon coupling).[13] The change in lattice parameter between LiH and LiD is known to be $\Delta a/a = -4\times10^{-3}$. The corresponding value for ^{6}Li→^{7}Li substitution is apparently unavailable, but could be expected to lie close to the value $\Delta a/a = -2.5\times10^{-4}$ observed for ^{6}LiF→^{7}LiF substitution. Assuming that the isotope shift is based essentially on these static $\Delta a/a$ variations, the ratio $(\Delta\nu/\nu):(\Delta a/a)$ for both Li^+ and H^- isotope variation is about -5. Comparable values of this ratio (measured under hydrostatic pressure) for F centers[14] are -3.5 ± 1.0. With the above assumption, these results indicate for our defect a very strong, F-center-like, dependence on the lattice spacing. Experiments under hydrostatic pressure are under way to test and confirm these assumptions and conclusions.

Under temperature increase from 10 to 80 K, the ZPL in LiH shifts by $\Delta\nu/\nu = -7.5\times10^{-4}$. Again under the assumption of a static origin of this effect and the validity of the above ratio of $(\Delta\nu/\nu):(\Delta a/a) = -5$, this would indicate a thermal lattice expansion between 10 and 80 K of 1.5×10^{-4}. This rather low value may indicate the presence of sizable dynamic contributions to the thermal shift, as observed in ZPL defects in alkali halides.[13]

The (lowest-energy) absorption spectrum of the defect in question should consist of the same zero-phonon line and a sideband spectrum at high energies, which is expected to be roughly a mirror image of the luminescence sideband spectrum.[13] Maximum efficiency of the luminescence is expected to occur for excitation into the peaks of this absorption sideband spectrum (about 560—580 nm range). Under variation of the exciting Ar^+-ion-laser line from 457 to 514 nm (corresponding to $\sim5000-2600$ cm^{-1} shift from the zero-phonon line) we found a steady increase of the luminescence intensity, indicating a far extending high-energy tail of this absorption.

As mentioned in Sec. III, the observed defect luminescence decreases strongly with temperature and changes into new luminescence spectra, consisting of at least two new zero-phonon lines (at 599.6 and 618.7 nm) and new sideband spectra. A systematic study into the nature and optical properties of these defects, which will involve variation in doping and defect production, as well as systematic absorption, polarization, and photochemical conversion measurements, is planned for a separate work.

TABLE V. Assignments of two-phonon spectra (300 K).

Peak number	Phonon frequencies (cm^{-1}) ^{7}LiH Observed	^{7}LiH Calculated[a]	^{7}LiD Observed	^{7}LiD Calculated[a]	Assignment Zone point	Assignment Phonon combinations
1	508	505	284	284	L	TO−TA
2	589	572	591	570	X	TA + TA
3	685	678	695	681	X	LA + TA
4	739	784	753	792	X	LA + LA
5	776		795			
6	1108	1107	907	874	X	TO + TA
7	1206	1213	968	985	X	TO + LA
		1212		940	L	LO + TA
8	1289	1212	1049	940	L	LO + TA
		1293		957	X	
9[b]	~1631	1642	1114	1178	X	TO + TO
10	1832	1717	1305	1224	L	LO + TO
		1758		1261	X	
11	2109	1936	1495	1378	L	LO + LO
		1874		1344	X	

[a]From Ref. 8.

[b]Peak no. 9 is not resolved at 300 K, but its frequency at this temperature has been estimated by applying a correction to its value at 10 K, equivalent to those observed for nearby peaks.

V. CONCLUDING REMARKS

In this paper we have described Raman and luminescence spectra of three isotopes of lithium hydride crystals. The two-phonon Raman spectra have been categorized by observing the frequency ratios for various isotopes, and a comparison with lattice-dynamics calculations allows identification of the main features as zone-edge (X or L points) combination modes (see Table V). The values for ^{6}LiH are documented for the first time. The presence of—so far unspecified—defects with weak electron-phonon coupling allowed us to observe, in their luminescence side bands, one-phonon spectra, which reproduce with amazing accuracy the phonon densities and their isotope effects. Besides acting as ideal "local probes" for unperturbed phonons, these defects display in their zero-phonon electronic transitions various interesting isotope effects, which we plan to study further in future work.

ACKNOWLEDGMENTS

We express our thanks to Mr. Matt DeLong for growing the crystals and Dr. Werner Gellermann for assistance in irradiating the samples. This work was supported by the National Science Foundation under Grants Nos. DMR-77-12675 and DMR-81-05332.

*Permanent address: Department of Physics, University of Waterloo, Waterloo, Ontario N2L 3G1, Canada.

[1]B. Gliss and H. Bilz, Phys. Rev. Lett. 21, 884 (1968).

[2]F. E. Pretzel, G. V. Gritton, C. C. Rushing, R. J. Friauf, W. B. Lewis, and P. Waldstein, J. Phys. Chem. Solids 23, 325 (1962), and three earlier papers from the same group cited in this reference.

[3]W. B. Zimmerman and D. J. Montgomery, Phys. Rev. 120, 405 (1959).

[4]A. S. Filler and E. Burstein, Bull. Am. Phys. Soc. 5, 198 (1960).

[5]M. W. Guinan and C. F. Cline, J. Nonmetals 1, 11 (1972).

[6]M. H. Brodsky and E. Burstein, in *Lattice Dynamics,* edited by F. R. Wallis (Pergamon, Oxford, 1965).

[7]M. G. Zemlianov, E. G. Brovman, N. A. Chernoplekov, and I. L. Shitikov, in *Inelastic Scattering of Neutrons* (IAEA, Vienna, 1965), Vol. 2, p. 431.

[8]J. L. Verble, J. L. Warren, and J. L. Yarnell, Phys. Rev. 168, 980 (1968).

[9]S. S. Jaswal, G. Wolfram, and T. P. Sharma, J. Phys. Chem. Solids 35, 571 (1974).

[10]R. Zeyher, Phys. Rev. Lett. 35, 174 (1975).

[11]G. Wolfram, S. S. Jaswal, and T. P. Sharma, Phys. Rev. Lett. 29, 160 (1972).

[12]L. Brillouin, *Wave Propagation in Periodic Structures* (Dover, New York, 1953).

[13]D. B. Fitchen, in *Physics of Color Centers,* edited by W. B. Fowler (Academic, New York, 1968).

[14]I. S. Jacobs, Phys. Rev. 93, 993 (1954).